Electrical Engineering Faculty Publications   Department of Electrical Engineering

10-1976

Ellipsometer nulling: convergence and speed

Rasheed M.A. Azzam
University of New Orleans, razzam@uno.edu

D. L. Confer

N. M. Bashara

Recommended Citation

D. L. Confer, R. M. A. Azzam, and N. M. Bashara, "Ellipsometer nulling: convergence and speed," Appl. Opt. 15, 2568-2575 (1976) http://www.opticsinfobase.org/ao/abstract.cfm?URI=ao-15-10-2568.

Ellipsometer nulling: convergence and speed

D. L. Confer, R. M. A. Azzam, and N. M. Bashara

The process of nulling in ellipsometry is studied by a graphical presentation using the trajectories of two significant polarization states in the complex plane, χ_{PC} and χ_{SA}. These states are determined by (1) the polarizer and compensator (χ_{PC}) and (2) the specimen and the analyzer (χ_{SA}) in the polarizer–compensator–specimen–analyzer ellipsometer arrangement. As the azimuth angles of the ellipsometer elements are varied, χ_{PC} and χ_{SA} move closer to one another in a stepwise fashion until they coincide when a null is reached. Thus, at null, the polarization states are matched, and $\chi_{PC} = \chi_{SA}$. For an isotropic reflector, the trajectory of χ_{SA} is a straight line, which simplifies the development of a criterion for achieving the most rapid nulling for two nulling procedures.

I.   Introduction

In this paper we treat the mode and speed of null convergence in ellipsometry where the azimuth of one of the three elements of the ellipsometer is held fixed and the azimuths of the other two elements are varied. The PCSA arrangement (polarizer, compensator, specimen, and analyzer) is assumed.[1] This investigation complements previous studies that have been concerned principally with the number of nulls available from a given arrangement and the conditions for nulling.[2] We also develop criteria and give examples for choosing azimuths of the fixed element to achieve rapid nulling with the fixed-compensator and fixed-polarizer arrangements. The optimum azimuths of the fixed elements to achieve rapid nulling are not necessarily the same as those that minimize various types of errors.[3,4]

Our presentation makes extensive use of trajectories of polarization states in the complex plane. This not only simplifies the complicated analytical processes involved, but also provides new insight in understanding the nulling process.

It is very interesting to observe the similarity between the nulling of an ellipsometer and the nulling of an ac bridge. In both cases, two elements are alternately adjusted until a null is reached. The null convergence curves for an ellipsometer in the complex polarization plane, which we introduce for the first time in this paper, are similar to the convergence curves of the ac voltage across the null detector of an ac bridge.[5]

The authors are with the University of Nebraska, Electrical Materials Laboratory, Engineering Research Center, Lincoln, Nebraska 68508.

II.   Complex Polarization States χ_{PC} and χ_{SA}

In Cartesian basis states, the Jones[6] vector $\mathbf{E}$ of a polarized light beam is

$$\mathbf{E} = \begin{bmatrix} E_x \\ E_y \end{bmatrix}, \qquad (1)$$

where E_x and E_y are the complex components of $\mathbf{E}$ along the x and y directions of a right-handed Cartesian coordinate system whose positive z axis is coincident with the direction of the beam. The polarization state χ of the vector $\mathbf{E}$ is defined by

$$\chi = E_y/E_x \qquad (2)$$

and is representable by a point in the complex plane.[7]

Two states of polarization will be used in the discussion that follows: the polarization state χ_{PC} that is incident on the specimen and the polarization state χ_{SA} that, if incident on the specimen, would be exactly extinguished by the linear analyzer, thus leading to zero output at the detector. In terms of the polarization-transforming properties of the elements of the PCSA ellipsometer, these states are

$$\chi_{PC} = \frac{\tan C - j \tan(P - C)}{1 + j \tan C \tan(P - C)}, \qquad (3)$$

and

$$\chi_{SA} = \frac{R_{pp} \tan(A - \pi/2) - R_{sp}}{R_{ss} - R_{ps} \tan(A - \pi/2)}, \qquad (4)$$

as can be proved by direct application of the Jones calculus.[2] In Eq. (3) P and C are the polarizer and compensator azimuth angles, and in Eq. (4) A is the analyzer azimuth, and $\mathbf{R} = (R_{ij})$ is the reflection matrix.

This paper focuses on the two polarization states χ_{PC} and χ_{SA} during the nulling process, these states being ultimately matched at null:

$$\chi_{PC} = \chi_{SA}. \qquad (5)$$

Fig. 1. Family of fixed-compensator, variable-polarizer contours (dashed lines) and fixed-polarizer, variable-compensator contours (solid lines) in the complex plane. These contours represent the trajectories of the polarization state χ_{PC} incident on the specimen when either the polarizer or compensator is held at fixed azimuth angle, and the other element is rotated. For example, the arrows indicate how the double-lobed trajectory χ_{PC} for a fixed-polarizer azimuth of 30° is traced as the compensator azimuth is varied.

III. Theory of Null Convergence

A. Trajectories of the Polarization States χ_{PC} and χ_{SA}

In ellipsometer nulling, the azimuth of one optical element is fixed. One of the other two elements is rotated to obtain a minimum in the output signal intensity, and this is followed by rotation of the second variable element to obtain a still lower output signal. Repeated alternate adjustments of the variable elements are made through a series of decreasing inten-

sity minima until the smallest minimum is reached and the signal intensity cannot be reduced further. This condition defines the null at a set of azimuth angles P_n, C_n, and A_n for the polarizer, compensator, and analyzer, respectively. Multiple nulls exist when the compensator or polarizer are held at a fixed azimuth,[2] and the azimuthal location of these nulls change when the azimuth of the fixed element is changed.

The contours[2] in Fig. 1 are members of the two families of contours associated with the polarization state χ_{PC} in Table I, where P or C is varying. The family of circles whose centers are located along the real axis of the complex plane are the fixed-compensator, variable-polarizer family[8] (dashed lines). The double-lobed contours (solid lines) in Fig. 1 are members of the fixed-polarizer, variable-compensator family.[9]

Figure 1 is a valuable graphical tool for the study of ellipsometer nulling. When doing fixed-compensator, variable-polarizer or fixed-polarizer, variable-compensator nulling, the state χ_{PC} is restricted to the appropriate contour of Fig. 1, and nulls will exist where this contour intersects the specimen-analyzer contour of Table I. This fact alone enables one to determine, with only limited knowledge of a specimen, how many nulls are available and approximately where they will be located. In addition, we shall show in Sec. III.D that considerable information regarding the speed of null convergence can be obtained directly from the complex-plane graph.

It will be helpful to first consider, by simulated calculations, the nature of the nulling process for the three schemes. Figure 2 gives an example of fixed-compensator nulling where the polarizer and analyzer are alternately varied (designated by the points P_1, A_1; P_2, A_2, etc.) to reach a null. The complete circle is χ_{PC}, and the segment of a circle is χ_{SA}. Figure 3

Table I. Equations of the Element Contours

Contour[a]	Variable azimuth	Polarization state in motion		Complex plane equation[b]
1a System-analyzer circle	A	χ_{SA}	where	$\chi_{SA}\chi_{SA}{}^* - \chi_{SA}\hat{C}^* - \chi_{SA}{}^*\hat{C} + \hat{C}\hat{C}^* - r^2 = 0$, $\hat{C} = \dfrac{T_{11}T_{22}{}^* - T_{21}T_{12}{}^*}{T_{22}T_{12}{}^* - T_{22}{}^*T_{12}}$ and $r = \dfrac{\lvert T_{11}T_{22} - T_{21}T_{12}\rvert}{2\lvert \mathrm{Imag}(T_{22}T_{12}{}^*)\rvert}$.
1b System-analyzer trajectory for isotropic reflectors (straight line) $T_{12} = T_{21} = 0$	A	χ_{SA}	where	$\chi_{SA}(\tan\Delta + j) + \chi_{SA}{}^*(\tan\Delta - j) = 0$, $\Delta = \arg T_{11} - \arg T_{22}$.
2 Fixed-compensator, variable-polarizer family of circles	P	χ_{PC}	where	$\chi_{PC}\chi_{PC}{}^* - \chi_{PC}\hat{C}^* - \chi_{PC}{}^*\hat{C} + \hat{C}\hat{C}^* - r^2 = 0$, $\hat{C} = -\cot 2C_f$, $r = \lvert \csc 2C_f \rvert$, and $-\pi/4 \leqslant C_f \leqslant +\pi/4$.
3 Fixed-polarizer variable-compensator family of contours	C	χ_{PC}	where	$(\chi_{PC} - \tan P_f)^2(1 + \chi_{PC}{}^{*2}) + (\chi_{PC}^* - \tan P_f)^2(1 + \chi_{PC}{}^2) = 0$, $0 \leqslant P_f \leqslant \pi$.

[a] For fixed-compensator nulling use contours 1 and 2, for fixed-polarizer nulling use contours 1 and 3, for fixed-analyzer nulling use contours 2 and 3.
[b] The complex conjugate is indicated by an asterisk (*). The center of a circle is given by the complex number $\hat{C}$; the radius is given by the real number r. Vertical bars (|) denote the magnitude of the enclosed complex number.
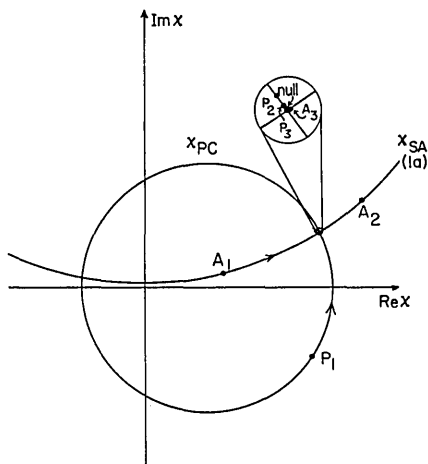
Fig. 2. An example of fixed-compensator nulling where the polarizer and analyzer azimuths are varied to obtain a null. The complete circle is the χ_{PC} contour (the fixed-compensator, variable-polarizer circle of Fig. 1), and the circle arc is the χ_{SA} contour. Here and throughout, the number below χ_{PC} or χ_{SA} identifies the corresponding appropriate expression in Table I. The nulling sequence is started with the state A_1 on the χ_{SA} trajectory and the state P_1 on the χ_{PC} trajectory. Alternate adjustments of analyzer and polarizer move the states, on their respective trajectories, to A_2, P_2; P_3, A_3, etc. to the null.
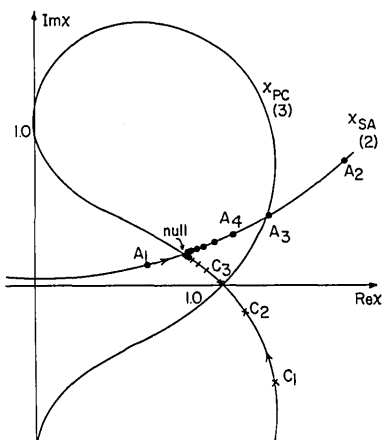
Fig. 3. An example of fixed-polarizer nulling. In this case χ_{PC} is represented by the double-lobed contour, and χ_{SA} is as in Fig. 2. Alternate adjustments of the compensator and analyzer azimuth angles result in the succession of states on the appropriate contours, A_1, C_1; A_2, C_2, etc. to the null.

shows null convergence when the polarizer is at a fixed azimuth angle. The circle arc is χ_{SA}, and the double-lobed contour is χ_{PC}. The compensator and analyzer azimuths are alternately varied (points A_1, C_1; A_2, C_2, etc.) to obtain a null. Finally, in Fig. 4 we show an example of fixed-analyzer nulling. We start with χ_{PC} at the point marked 11 where the polarizer and compensator are at their initial azimuths. The polarizer is held fixed, and the compensator is varied until χ_{PC} reaches point 12. Then, the compensator is fixed, the polarizer is varied to reach point 22, etc. In this manner, χ_{PC} is brought successively closer to

the state χ_{SA}, which is represented by a fixed point, until these two polarizations are finally matched (χ_{PC} = χ_{SA}) at null.

B. Relation Between Output Intensity and Trajectories of χ_{PC} and χ_{SA}

Consider a totally polarized light wave with an arbitrary electric vector **E** and intensity I, which is represented as the sum of two orthogonal vectors $\mathbf{E}_1$ and $\mathbf{E}_2$. The orthogonality condition of $\mathbf{E}_1$ and $\mathbf{E}_2$ is

$$\mathbf{E}_1^\dagger \mathbf{E}_2 = \mathbf{E}_2^\dagger \mathbf{E}_1 = 0, \tag{6}$$

where the Hermitian conjugate is indicated by the dagger ($\dagger$). This is equivalent to the condition that[7]

$$\chi_1 \chi_2^* = \chi_1^* \chi_2 = -1, \tag{7}$$

where χ_1 and χ_2 are the complex polarization states of $\mathbf{E}_1$ and $\mathbf{E}_2$, respectively, and the asterisk (*) indicates the complex conjugate. The intensity of the vector **E** can be written as

$$I = \eta_1 I + \eta_2 I, \tag{8}$$

where η_1 and η_2 are the fractions of the total intensity of **E** contained in the components $\mathbf{E}_1$ and $\mathbf{E}_2$, and

$$\eta_1 + \eta_2 = 1. \tag{9}$$

Now consider the light vector $\mathbf{E}_{PC}$, leaving the polarizer-compensator section of the ellipsometer, whose intensity and associated complex polarization state are I_{PC} and χ_{PC}, respectively. We resolve $\mathbf{E}_{PC}$ into orthogonal components $\mathbf{E}^1_{PC}$ and $\mathbf{E}^2_{PC}$ with complex polarization states χ_{SA} and χ°_{SA}, where χ°_{SA} is the state orthogonal to the state χ_{SA}. The component $\mathbf{E}^1_{PC}$, polarized in the state χ_{SA}, will be extinguished by the specimen–analyzer combination. This is the condition by which χ_{SA} was defined in Eq. (4). On the other hand, the wave $\mathbf{E}^2_{PC}$ polarized in the state χ°_{SA} will be passed with maximum transmittance by the specimen–analyzer combination. We can write the intensity incident on the photodetector as
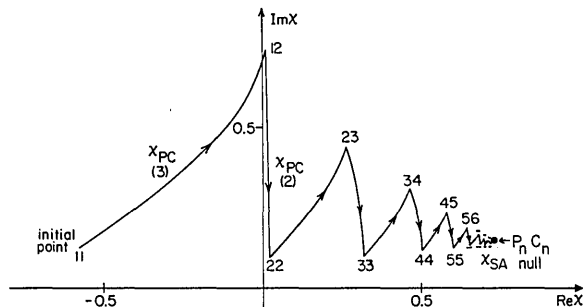
Fig. 4. Fixed-analyzer nulling. From the initial state 11 to the state 12 χ_{PC} moves along a segment of a fixed-polarizer, variable-compensator double-lobed contour; from 12 to 22 χ_{PC} moves on an arc of a fixed-polarizer, variable-compensator circle. Alternate adjustments of polarizer and compensator azimuths always result in a null.
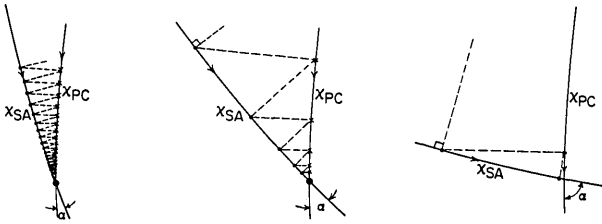
Fig. 5. An exploded view near the null as α, the angle of separation between χ_{PC} and χ_{SA}, increases from left to right. In the text we show that the angle α is an indicator of the speed of nulling.

$$I_D = \eta_2 I_{PC} = (1 - \eta_1)I_{PC}. \tag{10}$$

The fractions of intensity η_1 and η_2 are functions of the complex polarization states χ_{PC} and χ_{SA} only[10]

$$\eta_1 = \frac{1 + \chi_{PC}\chi^*_{SA} + \chi^*_{PC}\chi_{SA} + \chi_{PC}\chi^*_{PC}\chi_{SA}\chi^*_{SA}}{1 + \chi_{PC}\chi^*_{PC} + \chi_{SA}\chi^*_{SA} + \chi_{PC}\chi^*_{PC}\chi_{SA}\chi^*_{SA}}, \tag{11}$$

and

$$\eta_2 = \frac{\chi_{PC}\chi^*_{PC} - \chi^*_{PC}\chi_{SA} - \chi_{PC}\chi^*_{SA} + \chi_{SA}\chi^*_{SA}}{1 + \chi_{PC}\chi^*_{PC} + \chi_{SA}\chi^*_{SA} + \chi_{PC}\chi^*_{PC}\chi_{SA}\chi^*_{SA}}. \tag{12}$$

Either Eq. (11) or Eq. (12) together with Eq. (10) provide the connection between the polarization states χ_{PC} and χ_{SA} in the complex plane and the output intensity of the ellipsometer. In each nulling step, when one polarization state χ_{PC} or χ_{SA} changes, the intensity output can be minimized by maximizing Eq. (11) or by minimizing Eq. (12).

C. Nearness Function

It is convenient to define a nearness function[11], $N(\chi_{SA}, \chi_{PC})$, which has a particularly simple complex-plane interpretation:

$$N(\chi_{SA}, \chi_{PC}) = \left(\frac{\eta_2}{\eta_1}\right)^{1/2}$$

$$= \left(\frac{\chi_{PC}\chi^*_{PC} - \chi^*_{PC}\chi_{SA} - \chi_{PC}\chi^*_{SA} + \chi_{SA}\chi^*_{SA}}{1 + \chi_{PC}\chi^*_{SA} + \chi^*_{PC}\chi_{SA} + \chi_{PC}\chi^*_{PC}\chi_{SA}\chi^*_{SA}}\right)^{1/2}. \tag{13}$$

To relate the detected intensity I_D to the above nearness function, we substitute from Eqs. (12) and (13) into Eq. (10)

$$I_D = \frac{N^2(\chi_{SA}, \chi_{PC})}{1 + N^2(\chi_{SA}, \chi_{PC})} \cdot I_{PC}. \tag{14}$$

Equation (14) shows that the detected intensity will be minimized when $N(\chi_{SA}, \chi_{PC})$ is a minimum. Equation (13) can be cast in the form

$$N(\chi_{SA}, \chi_{Pc}) = \frac{|\chi_{SA} - \chi_{PC}|}{|\chi_{SA}| \cdot |\chi^0_{SA} - \chi_{PC}|}, \tag{15}$$

where the bars denote the magnitude of the enclosed complex number. The significance of this expression lies in its simple graphical interpretation. The nearness function $N(\chi_{SA}, \chi_{PC})$ (overlooking the factor

$1/|\chi_{SA}|$) is determined by the ratio of the distance between χ_{PC} and χ_{SA} to the distance between χ_{PC} and χ^0_{SA}. Because $N(\chi_{SA}, \chi_{PC}) = N(\chi_{PC}, \chi_{SA})$ [Eq. (13)], Eq. (15) can also be written as

$$N(\chi_{SA}, \chi_{PC}) = \frac{|\chi_{PC} - \chi_{SA}|}{|\chi_{PC}| \cdot |\chi^0_{PC} - \chi_{SA}|}. \tag{16}$$

It is convenient to use Eq. (15) when χ_{PC} changes, and χ_{SA} and χ^0_{SA} are fixed in the complex plane. Equation (16) is useful when χ_{SA} varies, and χ_{PC} and χ^0_{PC} are fixed. These relations can be studied either numerically or graphically.

D. Speed of Nulling

Consider Eq. (15) in the vicinity of the null. It can be shown that the numerator varies much more rapidly than the denominator.[12] Therefore,

$$N(\chi_{SA}, \chi_{PC}) \propto |\chi_{SA} - \chi_{PC}|. \tag{17}$$

Thus, to a first approximation, the nearness function and, therefore, the intensity are at a minimum when the distance between χ_{SA} and χ_{PC} is minimum. This result provides a simple procedure for the determination of near-null convergence. During each nulling step, one of the two points χ_{PC} or χ_{SA} is fixed and the other moves until the distance $|\chi_{PC} - \chi_{SA}|$ is minimum, at which point the step is completed. When χ_{PC} and χ_{SA} trace two fixed contours, the condition of minimum distance corresponds to drawing a line from a point on one contour perpendicular to the other. Figure 5 shows χ_{SA} and χ_{PC} contours with varying degrees of angular separation as measured by the angle α. When α is small [Fig. 5 (left)], a large number of steps are needed before the null is reached, which is in contrast to the case when α is large [Fig. 5 (right)]. Near null, we can use a straight-line approximation for the contours of χ_{PC}
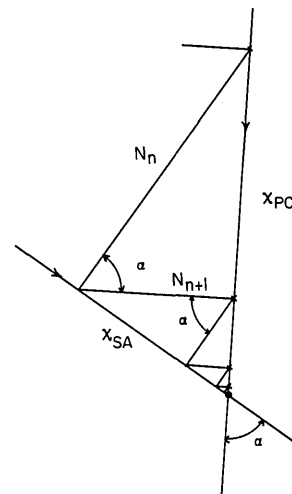
Fig. 6. A geometrical construction required for the derivation of Eq. (19).
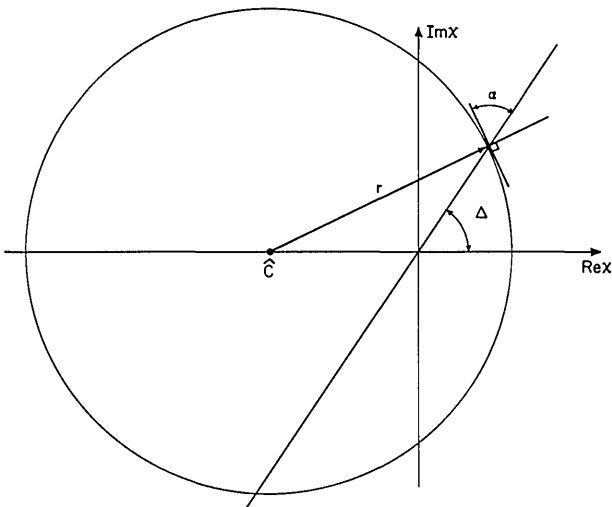
Fig. 7. The geometry for determining the angle α in the fixed-compensator nulling scheme for an isotropic reflector. The center ($\hat{C}$) and radius (r) of the fixed-compensator, variable-polarizer circle, from Table I, are $-\cot 2C_f$ and $|\csc 2C_f|$, respectively.

and χ_{SA} (Fig. 6). With this approximation and from Eq. (17) and the geometry of Fig. 6, we have

$$\frac{N(\chi_{SA}, \chi_{PC})|_{n+1}}{N(\chi_{SA}, \chi_{PC})|_n} = \frac{|\chi_{SA} - \chi_{PC}|_{n+1}}{|\chi_{SA} - \chi_{PC}|_n} = \cos \alpha. \quad (18)$$

Consequently, from Eq. (14), the ratio of the intensities at the $(n + 1)$th and nth successive minima is given by

$$\frac{I_{n+1}}{I_n} = \frac{N^2_{n+1}}{N^2_n} \frac{1 + N^2_n}{1 + N^2_{n+1}} \approx \frac{N^2_{n+1}}{N^2_n} = \cos^2 \alpha. \quad (19)$$

In Eq. (19) we have dropped the function arguments from N. From Eq. (19), we see that the rate of decrease in intensity is proportional to the cosine squared of the angle α. When α is greater than 60°, the intensity decreases by a factor greater than 4 on each step, and convergence to the null is very rapid. Conversely, when α is less than 45°, the intensity decreases by a factor less than 2 on each step, which is characteristic of slowly convergent nulling.

The approximations made above become more exact as the null is approached. The angle α is an indicator of how rapidly a null will be reached.

IV. Speed of Nulling for Isotropic Reflectors— Discussion and Examples

Isotropic reflectors are characterized by zero $p \leftrightarrow s$ cross-reflection coefficients. Their reflection Jones matrix is

$$\mathbf{R} = \begin{bmatrix} R_{pp} & 0 \\ 0 & R_{ss} \end{bmatrix}. \quad (20)$$

From ellipsometric measurements on such surfaces, one obtains the familiar ratio

$$R_{pp}/R_{ss} = \tan \psi \exp(j\Delta), \quad (21)$$

where $\tan \psi$ is the ratio of the p amplitude-reflection coefficient to the s amplitude-reflection coefficient, and Δ is the relative p-to-s phase shift.

In the complex plane, the polarization state χ_{SA} associated with an isotropic reflector traces a straight line that passes through the origin of the complex plane and has a slope $\tan \Delta$.[13] The straight-line trajectory of χ_{SA} simplifies the nulling analysis considerably.

A. Fixed-Compensator Nulling

When the compensator is fixed, the state χ_{PC} is free to move along the appropriate fixed-compensator, variable-polarizer circle in Fig. 1. The angle of intersection α between this circle of χ_{PC} and the straight line of χ_{SA} is

$$\alpha = 90° - \arcsin(\sin \Delta \cdot |\cos 2C_f|), \quad (22)$$

where C_f is the fixed-compensator azimuth. The derivation of Eq. (22) is based on Fig. 7, where the straight line of χ_{SA} is shown intersecting the circle of χ_{PC}. From the law of sines

$$\frac{\sin(90° - \alpha)}{|\cot 2C_f|} = \frac{\sin(180° - \Delta)}{|\csc 2C_f|}.$$

With the application of trigonometric identities, this expression reduces to Eq. (22), which can be used to predict the nulling speed of the fixed-compensator scheme for any isotropic reflector. Figure 8 plots curves of constant α vs C_f and Δ. For combinations of C_f and Δ which lie outside the curve $\alpha = 60°$, null convergence will be rapid [see discussion associated with Eq. (19)]. For combinations lying inside the curve $\alpha = 45°$, convergence will be slow. Thus, with a rough estimate of the value of Δ for a given specimen, Fig. 8 allows one to pick the fixed-compensator azimuths C_f, which give rapid null convergence.

The fastest null convergence occurs when $\alpha = 90°$.
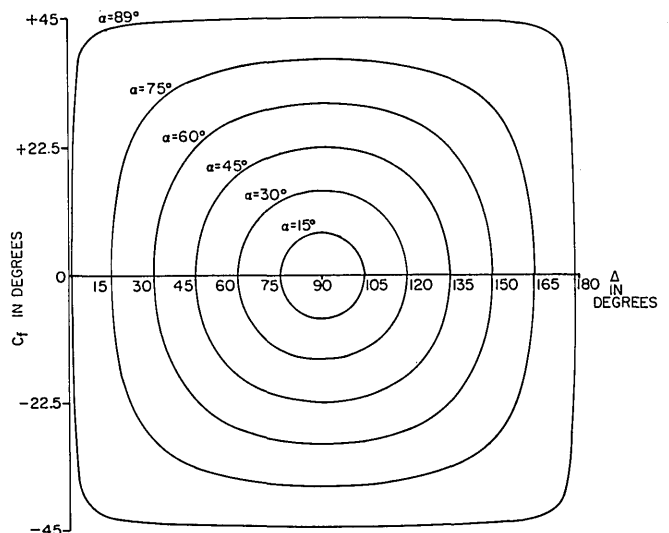
Fig. 8. Contours of constant α for fixed-compensator nulling. Combinations of C_f and Δ outside of $\alpha = 60°$ lead to rapid nulling.
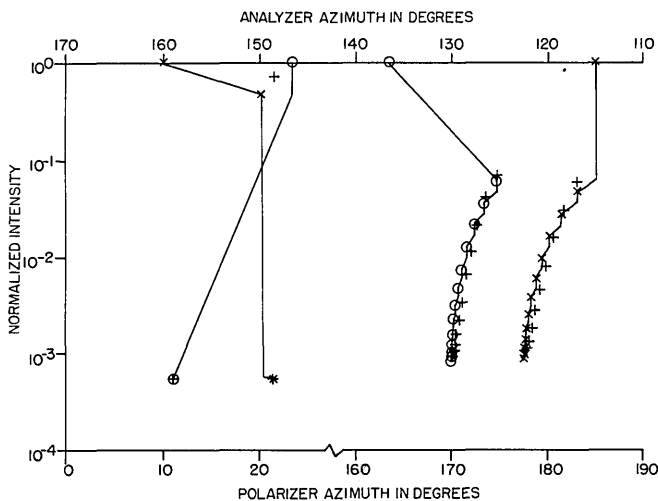
Fig. 9. Speed of nulling for two examples where the compensator is held at fixed azimuth. At the left of the figure, the compensator is at +45°; to the right of the figure the compensator is at 10°. The circles (O) are the measured polarizer azimuths, the crosses (X) are the measured analyzer azimuths. The computed points are marked with plus signs (+). For this example, using a gold film, it can be seen that the number of steps to a null is considerably less for the compensator azimuth of +45°.

α becomes 90° under two conditions, which are found from Eq. (22) as

$$\Delta = 0° \text{ or } 180°, \quad -45° \leq C_f \leq 45°, \quad (23)$$

and

$$C_f = \pm 45°, \quad 0° \leq \Delta \leq 180°. \quad (24)$$

Equation (23) describes reflection from a perfect dielectric with the compensator fixed at an arbitrary azimuth. (In this case, the compensator is actually not needed.) Equation (24) describes reflection from an arbitrary isotropic specimen with the compensator fixed at ±45°. In either case, the angle α becomes 90°, and very rapid convergence is achieved. In fact, a single adjustment of the polarizer followed by a single adjustment of the analyzer is all that is required for a null under either of these situations. (This explains an important advantage of this commonly chosen setting of the compensator.) This can be proved as follows.

Consider the polarization states χ_{SA} and χ_{PC} to be arbitrarily positioned on their respective contours. Because the contour of χ_{SA} is a straight line through the origin, the state $\chi°_{SA}$, orthogonal to χ_{SA}, will be located at some point on this straight line [Eq. (7)]. The nearness of the states χ_{PC} and χ_{SA} will be at a minimum when χ_{PC} is located exactly at the intersection of the fixed-compensator, variable-polarizer circle and the system (surface)-analyzer straight line. When the polarizer is adjusted, the state χ_{PC} will move to the null location regardless of the state χ_{SA}. A subsequent adjustment of the analyzer will carry the state χ_{SA} to χ_{PC}, and the null condition [Eq. (5)] is reached. If the analyzer is adjusted first, an additional step is needed to reach a null.

To verify the above theory and illustrate its usefulness, ellipsometric measurements were taken on an isotropic gold specimen. An estimate for Δ was obtained from a single null measurement with the compensator azimuth fixed at 45°. In this case Δ is given by

$$\Delta = 90° - 2P_n + 180°·k, \quad (25)$$

where P_n is the polarizer azimuth at the null, and k is an integer chosen so that $0° \leq \Delta < 180°$.[14] From the null azimuth $P_n = 101.10°$, the approximate Δ value was found to be 67.80°. Based on this value of Δ, fixed-compensator measurements were performed with $C_f = 45°$ and with $C_f = 10°$. The first of these was chosen to give very rapid convergence, while the second illustrates slow convergence. In performing these measurements, the relative intensity and the element azimuths were recorded at each secondary minimum on the way to the null. The nulling data obtained were compared to numerically generated data based on the nulling theory of Sec. III. The results of the fixed-compensator nulling are shown in Fig. 9. As expected, three-step null convergence was obtained when the analyzer was adjusted first with $C_f = 45°$. This is in contrast to the case where $C_f = 10°$, which required twenty-six steps. In both cases, we note that the experimental results agree well with those predicted by theory. The computed intensities tended to be lower than the observed; this was due to the assumed ideal nature of the elements. To compensate partially for this effect, a linear correction was applied to the computed data.

B. Fixed-Polarizer Nulling

With the polarizer fixed, the state χ_{PC} is restricted to move along one of the fixed-polarizer, variable-compensator double-lobed contours of Fig. 1, while χ_{SA} moves along the system-analyzer straight line. The study of fixed-polarizer nulling convergence is complicated by the increased number of nulls available and the complex shape of the χ_{PC} contour in
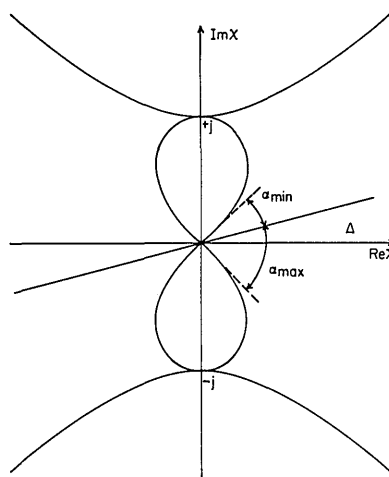
Fig. 10. The values of α_{min} and α_{max} for Δ in the range $0° < \Delta \leq 45°$. When Δ is between 135° and 180°, α_{min} and α_{max} are $\Delta - 135°$ and $225° - \Delta$, respectively.
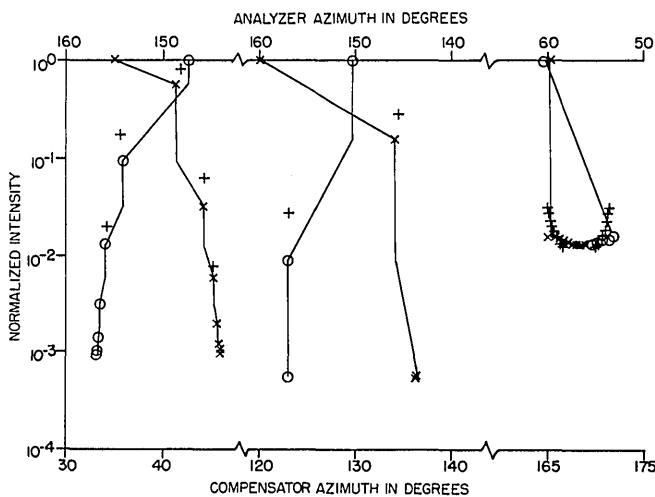
Fig. 11. Speed of nulling for three fixed-polarizer examples. At the left of the figure, the fixed-polarizer azimuth was $\approx 0.0°$, in the center it was 64.9°, and on the right the fixed-polarizer azimuth was 10.0°. The circles (O) are the measured compensator azimuths, the crosses (X) are the measured analyzer azimuths. The computed points are marked with plus signs (+). The central set of data illustrates rapid convergence, while the set on the left illustrates slower convergence. The set of data at the right shows convergence to a pseudonull.

this case. While an expression for the angle of contour intersection has not been derived, some general observations can be made regarding the speed of null convergence.

(1) For a perfect dielectric, $\Delta = 0°$ or $180°$, the angle α is always 45°. This is true for all fixed polarizer azimuths P_f.

(2) For the ranges $0° < |\Delta| \leq 45°$ and $135° \leq |\Delta| < 180°$, two nulls are found on each fixed-polarizer contour. For either null, α will lie between the extremes α_{min} and α_{max} (see Fig. 10). These extremes will occur when $P_f = 0°$ or $90°$ and are given by

$$\alpha_{max} = 45° + \Delta - 180 \cdot k \qquad (26)$$

and

$$\alpha_{min} = 45° - \Delta + 180 \cdot k, \qquad (27)$$

where $k = 0$ for $0° < |\Delta| \leq 45°$ and $k = 1$ for $135° \leq |\Delta| < 180°$. When $|\Delta| = 45°$ or $135°$, α_{min} and α_{max} are 0° and 90°, respectively.

(3) When Δ is in the range $45° < |\Delta| < 135°$, α values may range from 0° to 90°. A maximum of four nulls are available for each fixed azimuth P_f, and each of these may have a different α value. In general, four values of P_f in the range from 0° to 180° may be found for which $\alpha = 0°$ on one null out of the three that become available. Four other values of P_f may be found for which $\alpha = 90°$ on at least one null. These are

$$P_{f1} = \arctan[(-\cos 2\Delta)^{1/2}/\cos\Delta], \qquad (28a)$$

$$P_{f2} = 90° - P_{f1}, \qquad (28b)$$

$$P_{f3} = 180° - P_{f1}, \qquad (28c)$$

and

$$P_{f4} = 90° + P_{f1}. \qquad (28d)$$

For each of the four χ_{PC} contours that correspond to Eqs. (28), from one to three other nulls will be found with values of α other than 90°. Equations (28) can be proven[15] from the contour equations in Table I.

We performed fixed-polarizer nulling on the same gold specimen with $P_f = 64.9°$, 0.0°, and 10°. Since multiple nulls are available, some care was exercised in choosing initial azimuth values to insure convergence to the desired null. The first fixed polarizer azimuth, 64.9°, was chosen on the basis that at least one null of the two available would then provide rapid convergence [Eq. (28a)]. The other two fixed azimuths were chosen to show slow convergence and pseudonull convergence, respectively. A pseudonull describes an absolute minimum that is not a null but arises when the contours pass near to each other yet do not intersect. The ability to avoid pseudonulls during measurements is extremely important in the fixed-polarizer scheme.

In Fig. 11 the results of fixed-polarizer nulling are displayed and are as expected. The rapid convergence at $P_f = 64.9°$ as contrasted with $P_f \approx 0.0°$ is ample demonstration of the usefulness of Eqs. (28) for selecting fixed azimuth values. The sequence leading to pseudonull convergence when P_f was 10° suggests that these nulls are characterized by slow convergence and higher-than-normal null intensity. In the limit, however, as the pseudonull approaches the real null (the contours are nearly tangent), the higher intensity will not be evident. Such a pseudonull could only be detected by its extremely slow convergence. We can generalize and say that a null is a possible pseudonull wherever (a) the null intensity is unusually large or (b) the null convergence is extremely slow.
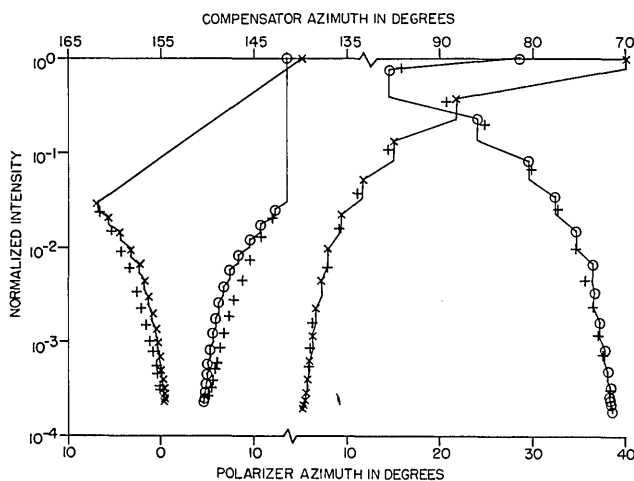
Fig. 12. Speed of nulling for two fixed-analyzer examples. For the data at the left of the figure, the analyzer azimuth was fixed at 40°; for the data at the right, the analyzer azimuth was fixed at 130°. The circles (O) are the measured polarizer azimuths, the crosses (X) are the measured compensator azimuths. The computed points are marked by plus signs (+). Both of these examples show the slow convergence inherent in the fixed-analyzer scheme.

C. Fixed-Analyzer Nulling

The speed of nulling in the constant-analyzer scheme is essentially independent of the system under test. The angle of contour intersection α is never greater than 45°, and, therefore, the process is relatively slow. The extent to which the system does affect the speed of nulling depends only on the location of the stationary state χ_{SA} in the complex plane (see Fig. 4). For example, if the system under study is a perfect dielectric ($\Delta = 0°$ or 180°), the stationary state χ_{SA} will lie on the real axis of the complex plane for all fixed-analyzer azimuths, and the angle of contour intersection is always 45°, the maximal angle. For other relative phase retardations, the angle α will vary somewhat depending on the fixed-analyzer azimuth.

We performed fixed-analyzer nulling at $A_f = 40°$ and at $A_f = 130°$. These azimuths were chosen arbitrarily to illustrate the relatively slow nature of the fixed-analyzer scheme. The results shown in Fig. 12 clearly support our predictions. The slow convergence of this nulling scheme is compensated for by the fact that the scheme will always converge to a single null.

V. Summary and Conclusions

The theory of ellipsometer nulling has been considered in detail, with particular emphasis on graphical display, and is applicable to any nulling scheme that uses a quarter-wave compensator and in which one element azimuth is fixed while the other two element azimuths are adjusted for the null. From the nulling theory, criteria are developed to judge the rate of null convergence. In particular, it is shown that the angle of intersection between the contours of two important polarization states in the complex plane is the primary factor in the rate of null convergence. When this angle is near 90°, rapid convergence is obtained.

The application of nulling theory to conventional ellipsometry has been considered. The rate of null convergence is compared for each of the three nulling schemes: fixed-compensator, fixed-polarizer, and fixed-analyzer. Expressions for obtaining rapid convergence are given for the fixed-compensator and the fixed-polarizer nulling schemes. Experimental results verify the theory of nulling.

References

1. The retardance of a compensator can also be used as a nulling variable. However, we are not considering this procedure in this paper.
2. R. M. A. Azzam and N. M. Bashara, J. Opt. Soc. Am. **62**, 336 (1972); Opt. Commun. **5**, 5 (1972); **7**, 110 (1973) (with T. L. Bundy).
3. E. Schmidt, J. Opt. Soc. Am. **60**, 490 (1970).
4. R. M. A. Azzam and N. M. Bashara, J. Opt. Soc. Am. **62**, 700 (1972).
5. W. Kidwell, *Electrical Instruments and Measurements* (McGraw-Hill, New York, 1969).
6. R. C. Jones, J. Opt. Soc. Am. **31**, 488 (1941).
7. R. M. A. Azzam and N. M. Bashara, J. Opt. Soc. Am. **62**, 222 (1972).
8. When the azimuth of the compensator is fixed at some value C_f, the polarization state χ_{PC} is restricted to motions along a single member of the fixed-compensator family. For example, when the compensator is fixed at 45°, the polarization state χ_{PC} is restricted to motions along the unit circle centered at the origin of the complex plane. For each fixed compensator azimuth, as the polarizer is rotated so that P-C changes from $-45°$ to $+45°$, the polarization state χ_{PC} moves from $+j$, around the member circle, to $-j$. (See Ref. 2, first paper.)
9. When the polarizer azimuth is fixed, the state χ_{PC} is restricted to a single member of this family. As the compensator is rotated from 0° through 80°, χ_{PC} moves from a point on the negative imaginary axis around the fixed-polarizer contour in the direction indicated in Fig. 1. See Ref. 2, third paper.
10. R. M. A. Azzam and N. M. Bashara, Appl. Phys. **2**, 59 (1973). [An alternate derivation can be found in the M.Sc. Thesis of D. L. Confer, University of Nebraska (1973).]
11. This is different from, although related to, the nearness functions defined in Ref. 10.
12. If we let $\chi_{SA} - \chi_{PC} = \delta\chi$, Eq. (15) becomes

$$N(\chi_{SA}, \chi_{PC}) = |\delta\chi|/(|\chi_{SA}| \cdot |\chi_{SA}{}^{\circ} - \chi_{SA} + \delta\chi|).$$

In the vicinity of the null, $\delta\chi$ is small, and this expression can be written as

$$N(\chi_{SA}, \chi_{PC}) \approx |\delta\chi|/(|\chi_{SA}| \cdot |\chi_{SA}{}^{\circ} - \chi_{SA}|).$$

When χ_{PC} is in motion, the denominator of this expression is a constant, so that $N(\chi_{SA}, \chi_{PC}) \propto |\chi_{SA} - \chi_{PC}|$, which is Eq. (17).
13. From Eqs. (4), (20), and (21), the expression for the polarization state χ_{SA} for an isotropic reflector becomes $\chi_{SA} = \tan(A - \pi/2) \tan\psi \exp(j\Delta)$. Thus all possible values of χ will lie on a straight line passing through the origin of the complex plane with a slope $\tan\Delta$.
14. R. M. A. Azzam and N. M. Bashara, J. Opt. Soc. Am. **61**, 600 (1971).
15. Equations (28) are derived by first noting that a 90° intersection will always occur when the fixed-polarizer contour P_{f1} intersects simultaneously the system-analyzer straight line and the fixed-polarizer contour $P_f = 0°$. We substitute $\chi_{PC} = |\chi_{PC}| \exp(j\Delta)$ into the fixed-polarizer equation Table I, with $\tan P_f = 0$. This allows one to solve for $|\chi_{PC}|$ in terms of Δ. With the value of χ_{PC} known, the general fixed-polarizer equation is solved for P_{f1}, yielding Eq. (28a). The additional azimuths P_{f2}, P_{f3}, and P_{f4} are found from symmetry considerations. For example, where the system-analyzer straight line crosses the $P_f = 90°$ contour, a second 90° intersection occurs with the contour P_{f2}. P_{f2}, however, need not be solved for directly because $P_{f2} = 90° - P_{f1}$. The two remaining angles are reflections of P_{f1} and P_{f2} in the right-hand side of the complex plane. They are $P_{f3} = 180 - P_{f1}$ and $P_{f4} = 180 - P_{f2} = 90 + P_{f1}$.